

# Linking the Jehol Biota evolution to the Early Cretaceous volcanism during the North China craton destruction: insights from F, Cl, S, and P

Qi-Hu Xu<sup>1</sup>, Lu WANG<sup>1</sup>, Jia Liu<sup>1</sup>, Etienne Deloule<sup>2</sup>, Eero Johannes Hanski<sup>3</sup>, Xiao-Yan Gu<sup>1</sup>, Huan Chen<sup>1</sup>, and Qunke Xia<sup>1</sup>

<sup>1</sup>Zhejiang University

<sup>2</sup>Université de Lorraine

<sup>3</sup>University of Oulu

November 22, 2022

## Abstract

The Early Cretaceous Jehol Biota evolution has remarkable spatiotemporal correlation with the destruction of the North China craton though the coupling mechanism remains enigmatic. The craton destruction was accompanied by intense magmatic activity and the released volatiles and nutrients might have had climatic and environmental impacts on the biotic evolution. In this study, we investigated the mentioned hypothetical causal link by determining concentrations and total emissions of volatile elements (S, F, Cl) and bulk-rock P contents of volcanic rocks that were erupted during the pre-flourishing, flourishing and post-flourishing stages of the Jehol Biota. Our results show that the volcanism near the flourishing stage has lower S (1083-2370 ppm), Cl (1277-5608 ppm) and higher P<sub>2</sub>O<sub>5</sub> contents (0.48-0.84 wt.%) than that in non-flourishing stages with S of 1991-3288 ppm, Cl of 7915-12315 ppm and P<sub>2</sub>O<sub>5</sub> of 0.17-0.23 wt.%. Fluorine contents in the three stages vary from 893 to 3746 ppm. The total volatile emissions are minor in the flourishing stage (3.6-6.6 Gt S, 2.2-4.6 Gt Cl and 2.1-4.0 Gt F) but elevated in the non-flourishing stages (1-690 Gt S, 4-934 Gt Cl and 1-308 Gt F). Our data suggest that regional climatic and environmental impacts of volcanism in the non-flourishing stages probably hindered the species diversification. The high P flux released from lithospheric mantle-derived lavas during the peak time of craton destruction might enhance primary productivity and contribute to the flourishing of the Jehol Biota. Our study provides insights into the relationship between the biosphere and deep geodynamic processes driven by volcanism.

## Hosted file

essoar.10511057.1.docx available at <https://authorea.com/users/533070/articles/598089-linking-the-jehol-biota-evolution-to-the-early-cretaceous-volcanism-during-the-north-china-craton-destruction-insights-from-f-cl-s-and-p>

**Linking the Jehol Biota evolution to the Early Cretaceous volcanism during the North China craton destruction: insights from F, Cl, S, and P**

**Qi-Hu Xu<sup>1</sup>, Lu Wang<sup>1\*</sup>, Jia Liu<sup>1\*</sup>, Etienne Deloule<sup>2</sup>, Eero Hanski<sup>3</sup>, Xiao-Yan Gu<sup>1</sup>, Huan Chen<sup>1</sup> and Qun-Ke Xia<sup>1</sup>**

<sup>1</sup>Key Laboratory of Geoscience Big Data and Deep Resource of Zhejiang Province, School of Earth Sciences, Zhejiang University, Hangzhou 310027, China

<sup>2</sup>Université de Lorraine, CNRS, CRPG, F-54000 Nancy, France

<sup>3</sup>Oulu Mining School, University of Oulu, P.O. Box 3000 90014 Oulu, Finland

\*Corresponding author: L. Wang and J. Liu, [wanglu9103@zju.edu.cn](mailto:wanglu9103@zju.edu.cn); [liujia85@zju.edu.cn](mailto:liujia85@zju.edu.cn)

Key Points:

- Volcanic gases (S, Cl and F) had limited climatic effects in the flourishing stage of the Jehol Biota
- High P flux from lithospheric mantle-derived lavas facilitated the flourishing of the Jehol Biota
- Volcanism associated with North China craton destruction affects terrestrial biota evolution

Abstract

The Early Cretaceous Jehol Biota evolution has remarkable spatiotemporal correlation with the destruction of the North China craton though the coupling mechanism remains enigmatic. The craton destruction was accompanied by intense magmatic activity and the released volatiles and nutrients might have had climatic and environmental impacts on the biotic evolution. In this study, we investigated the mentioned hypothetical causal link by determining concentrations and total emissions of volatile elements (S, F, Cl) and bulk-rock P contents of volcanic rocks that were erupted during the pre-flourishing, flourishing and post-flourishing stages of the Jehol Biota. Our results show that the volcanism near the flourishing stage has lower S (1083–2370 ppm), Cl (1277–5608 ppm) and higher P<sub>2</sub>O<sub>5</sub> contents (0.48–0.84 wt.%) than that in non-flourishing stages with S of 1991–3288 ppm, Cl of 7915–12315 ppm and P<sub>2</sub>O<sub>5</sub> of 0.17–0.23 wt.%. Fluorine contents in the three stages vary from 893 to 3746 ppm. The total volatile emissions are minor in the flourishing stage (3.6–6.6 Gt S, 2.2–4.6 Gt Cl and 2.1–4.0 Gt F) but elevated in the non-flourishing stages (1–690 Gt S, 4–934 Gt Cl and 1–308 Gt F). Our data suggest that regional climatic and environmental impacts of volcanism in the non-flourishing stages probably hindered the species diversification. The high P flux released from lithospheric mantle-derived lavas during the peak time of craton destruction might enhance primary productivity and contribute to the flourishing of the Jehol Biota. Our

study provides insights into the relationship between the biosphere and deep geodynamic processes driven by volcanism.

### **Plain Language Summary**

It is generally believed that volatiles, such as S, Cl and F, released by massive volcanic events may have strong ecological pressures both at the local and global scales. However, it is puzzling that the flourishing of the Jehol Biota, an Early Cretaceous terrestrial lagerstätte recording the origin and early evolution of feathered dinosaurs, birds, mammals and angiosperms, occurred simultaneously with the extensive volcanic activities in the northeastern China. To find the possible influence of volcanism on the biotic evolution, we determine the contents and total emissions of S, Cl and F (toxic gases) and bulk-rock P (nutrient) contents of volcanic rocks that were erupted during the pre-flourishing, flourishing and post-flourishing stages of the Jehol Biota. Our results show that the volcanism at the flourishing period of the Jehol Biota was dominated by intermediate-mafic magmas, the total S, Cl and F emissions of which had limited impacts on the local climate and environment, while the high P flux released from lavas might enhance primary productivity. On the contrary, the intermediate-felsic volcanic rocks in the non-flourishing stage released abundant toxic gases and the P flux was limited, which probably hindered the species diversification.

### **1 Introduction**

Volcanism provides an important mechanism transferring heat and matter (including volatiles and nutrient elements) from the Earth's interior to its surface reservoirs (Mather, 2015). Studies on the linkage between large igneous provinces (LIPs) and mass extinction events have shown that the volatiles, such as F, Cl and S, released by giant magmatic events can have strong global-scale effects on the biotic, environmental and climatic evolution (Sobolev et al., 2011; Callegaro et al., 2014; Oppenheimer et al., 2014). However, what are the effects of less extensive continental magmatism on the evolutionary history of regional biota remain largely unconstrained. Climate-modifying volcanic gases (CO<sub>2</sub>, SO<sub>2</sub> and halogens) may cause biota poisoning, environmental acidification, ozone depletion and climatic warming or cooling (Ernst & Youbi, 2017). In contrast, nutrients (e.g., P, Fe) derived from weathered lava flows can act as limiting factors for primary productivity in terrestrial and freshwater ecosystem (Elser et al., 2007; Augusto et al., 2017). The Jehol Biota, an Early Cretaceous terrestrial lagerstätte (Zhou et al., 2003), can be divided into different evolutionary stages encompassing its origin, development, flourish and decay (Zhou et al., 2021 and references therein). New geochronological data from the North China craton (NCC) on the spatiotemporal evolution of the Jehol Biota show that it coincided with the Cretaceous magmatism during the craton destruction (Zhu et al., 2020; Zhou et al., 2021). Although previous studies have emphasized the impacts of volcanism on the Jehol Biota, most of them focused on the role of volcanic ashes or pyroclastic flows causing mass mortality events and exceptional preservation of fossils (Jiang et al., 2014). In this study, we determined concen-

trations and total emissions of S, F and Cl as well as bulk-rock  $P_2O_5$  contents of volcanic rocks at the pre-flourishing (origin and development), flourishing and post-flourishing (decay) stages of the Jehol Biota, to examine the hypothetical causal link between the Early Cretaceous continental volcanic events and the Jehol Biota evolution. Together with compiled data from other volcanic events (i.e., LIPs and Toba), we discuss the impacts of the Early Cretaceous volcanism in the NCC on the terrestrial ecosystem and Jehol Biota evolution.

## 2 Geological setting and samples

The NCC is one of the oldest continental nuclei on Earth (Liu et al., 1992), which has lost its cratonic root through hydration-induced weakening, crustal delamination and/or mechanical erosion during the Mesozoic-Cenozoic (Wu et al., 2019 and references therein). The intensive magmatism and extensional deformation in the Cretaceous led to the development of widespread volcanic-sedimentary basins (Wu et al., 2005). In particular, the Early Cretaceous volcanic rocks are extensively distributed throughout the eastern and northern China.

The Jehol Biota is mainly distributed in the northern margin of the eastern NCC (including northern Hebei, western Liaoning and southeastern Inner Mongolia areas), and is primarily preserved in the Huajiying, Yixian, and Jiufotang Formations with ages spanning from 135 to 120 Ma (Figs. 1A-C; Pan et al., 2013). The Huajiying Formation contains fluvio-lacustrine and lacustrine siltstones interbedded with tuffs and tuffaceous clastics, recording the earliest occurrence of the Jehol Biota (ca. 135–127 Ma; Yang et al., 2020). The Yixian Formation (ca. 126–124 Ma), from bottom to top, consists of the Lujiatun Unit (fluvial tuffaceous, pebbly sandstones), Lower Lava Unit (basaltic to andesitic rocks), Jianshangou/Dawangzhangzi Unit (lacustrine shales and mudstones with tuff interlayers), Upper Lava Unit (andesitic to dacitic rocks), and Jingangshan Unit (lacustrine-facies clastics intercalated with rhyolitic pyroclastics) (Fig. 2A; Zhong et al., 2021). The Jianshangou Bed in the lower part of the Yixian Formation records the flourishing (with greatest species abundance and diversification) of the Jehol Biota as represented by nearly all Mesozoic plant groups (including angiosperms), insects, diverse birds, dinosaurs, pterosaurs, mammals, lizards, turtles, choristoderes, amphibians and fishes (Zhou et al., 2021). Compared with the Jianshangou Bed, the Jingangshan Bed in the upper part of the Yixian Formation contains significantly lower abundances and fewer species of fossils. The Jiufotang Formation is mainly composed of interbedded mudstones, siltstones, fine-grained sandstones and tuffs. The fossil assemblage preserved in the Lower Jiufotang Formation displays a remarkable differentiation of vertebrates between 123 Ma and 120 Ma (Yu et al., 2021; Zhou et al., 2021).

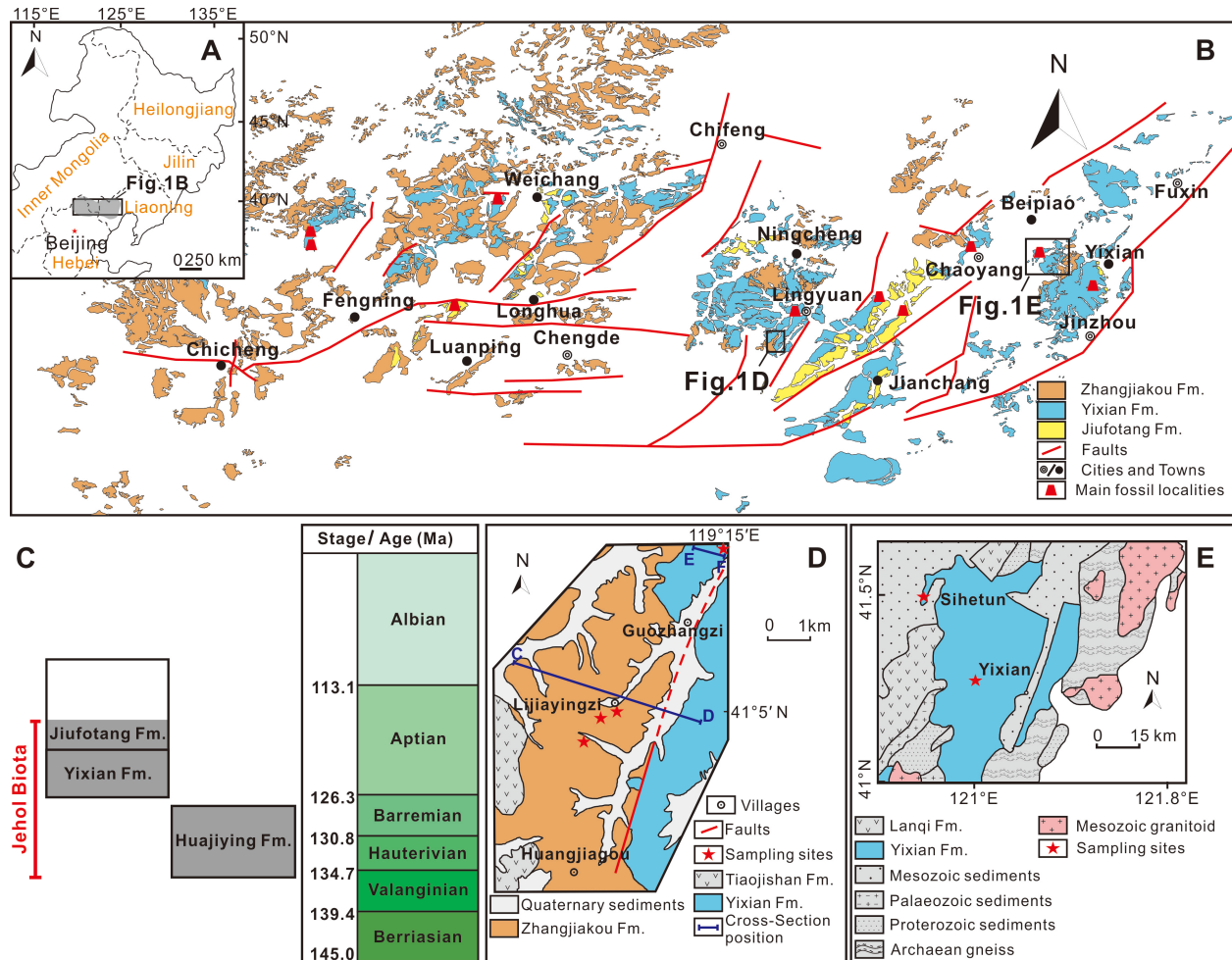


**Figure 1.** (A) Spatial distribution of the Jehol Biota in the northeastern North China craton (modified from Pan et al., 2013). (B) The main fossil localities of the Jehol Biota and the Early Cretaceous volcanic rocks in the western Liaoning, northern Hebei and southeastern Inner Mongolia (modified from Pan et al., 2013). (C) Lithostratigraphic and chronostratigraphic positions of the Jehol Biota (modified from Pan et al., 2013). (D) Geological map of the Dawangzhangzi-Maozishan district, Lingyuan and sampling sites (after Zhang et al., 2005). The cross-sections of C-D and E-F are the same with Zhang et al. (2005). (E) Geological map of the Yixian and Sihetun districts and sampling sites (after Geng et al., 2019). Fm. is the abbreviation of formation hereafter.

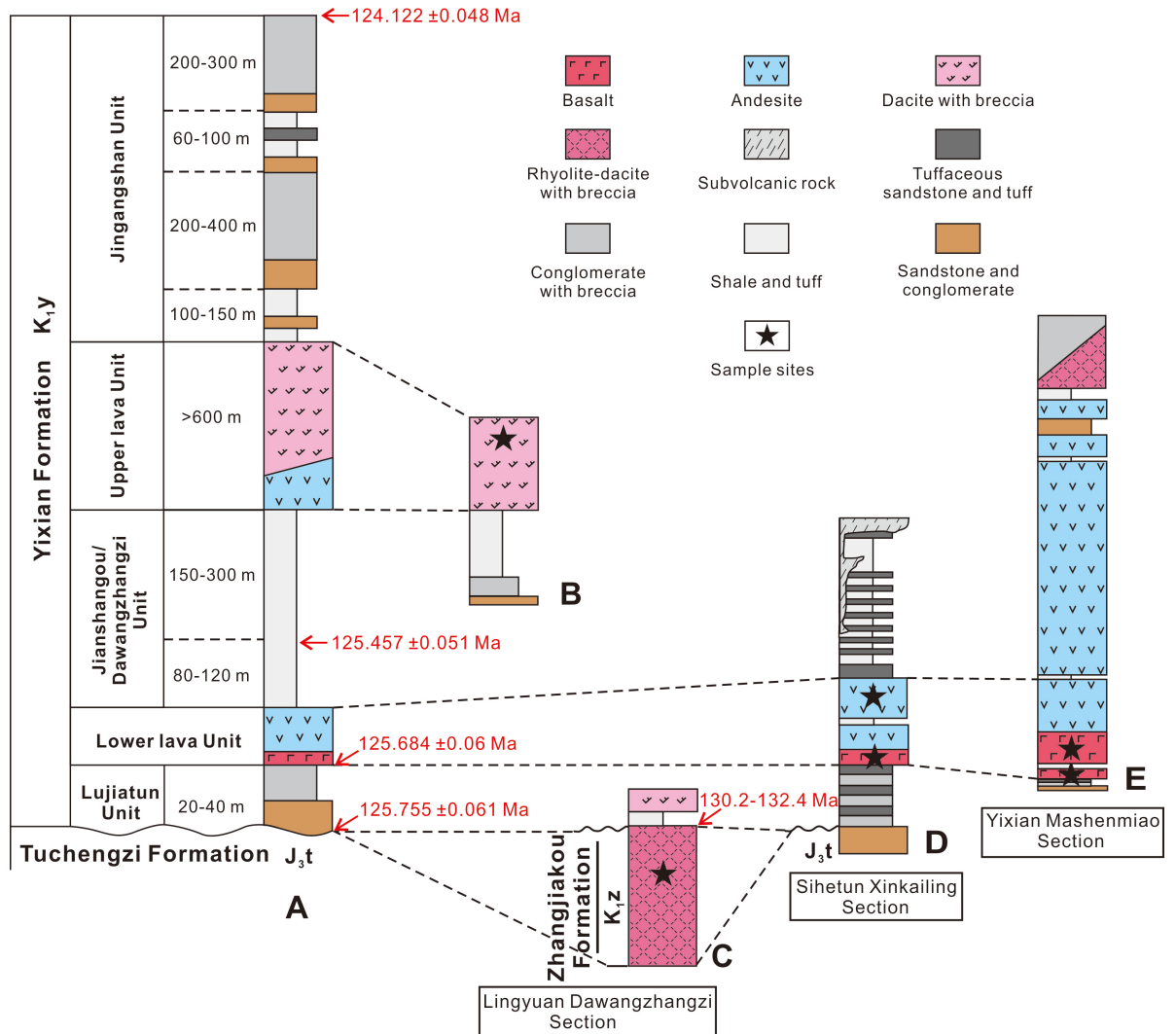


**Figure 2.** (A) Composite stratigraphic column of the Yixian Formation (modified from Zhong et al., 2021). (B)-(C) Stratigraphic columns of cross-sections C-D and E-F in Fig. 1D in the Lingyuan County. (D-E) Stratigraphic columns of the Xinkailing section in the Sihetun County, and the Mashenmiao section in the Yixian County (modified from Wang and Zhou, 2008).

The studied volcanic rocks were collected from the main fossil localities in the Lingyuan, Sihetun and Yixian Counties (Figs. 1D-E and 2), including three rhyolite samples of the Zhangjiakou Formation (~140-130 Ma felsic lavas; Yang et al., 2019), seventeen basalt samples (from both Yixian and Sihetun Counties) and four high-Mg andesite samples (HMAs) of the Lower Yixian Formation with ages between  $125.684 \pm 0.061$  Ma and  $125.457 \pm 0.051$  Ma (Zhong et al., 2021),

and one trachydacite sample of the Upper Yixian Formation with age between  $125.457 \pm 0.051$  Ma and  $124.122 \pm 0.048$  Ma (Zhong et al., 2021). Based on previous radiometric dating and stratigraphic correlation, the eruption ages of these volcanic rocks from the Zhangjiakou, Lower Yixian and Upper Yixian Formations overlapped with the pre-flourishing stage (I; origin and development), flourishing stage (II) and post-flourishing stage (III; decay) of the Jehol Biota, respectively. The volcanic rocks in the Jiufotang Formation are not considered in this study because they are mainly tuffs sourced from adjacent areas, while the local lavas are rare. Detailed sample descriptions are given in the Supporting text.

### 3 Methods

#### 3.1 Bulk-rock major-element analysis

Bulk-rock major-element analysis was conducted at ALS Chemex (Guangzhou, China) Co., Ltd. After removing the weathered surfaces, all samples were cut and ground into small fragments ( $<0.5$  cm in diameter). Then, they were cleaned with deionized water and ground to 200-mesh powder. The powder was divided into two parts. One part was dried and heated to  $1000$  °C in a muffle furnace. The loss-on-ignition (LOI) was determined by the weight loss before and after heating. The other part was dried at  $105$  °C and mixed with the compound flux of lithium tetraborate-lithium metaborate-lithium nitrate. Then, they were fused in a high-frequency melting furnace at  $1050$  °C. The melt was poured into a Pt crucible and cooled to form a thin fused glass disk. The major-element compositions were measured by an X-ray fluorescence spectrometer (XRF). The precision (relative standard deviation, RSD) was 1–3% for elements with concentrations of  $>1$  wt.% and  $\sim 10\%$  for those having concentrations of  $<1$  wt.%. The major-element compositions of the studied samples are given in Table S1.

#### 3.2 Pre-eruptive volatile content in magmas

##### 3.2.1 Method chosen for pre-eruptive volatile content measurement

A variety of methods have been proposed to quantify the pre-eruptive volatile contents of ancient volcanoes, including: (1) direct determination of volatile contents in volcanic glasses (Workman et al., 2006); (2) direct determination of volatile contents in melt inclusions (Wallace et al., 2021); and (3) indirect estimation of volatile contents in melts by combining the measured volatile concentrations in minerals with experimentally determined partition/exchange coefficients between minerals and melts (Xia et al., 2013; Callegaro et al., 2014; Liu et al., 2015). Given that the continental magmas tend to efficiently degas during their eruption, volcanic glass may record a much lower volatile content than the pristine value. In addition, melt inclusions in the continental volcanic rocks are rare and their volatile contents are easily modified during post-entrapment processes (Callegaro et al., 2014). Due to the absence of well-preserved melt inclusions, it is not appropriate to use the first two methods to estimate the volatile contents in our ancient ( $>100$  million years) continental volcanic sam-

ples. In this paper, we quantified the pre-eruptive S, Cl and F contents in melts by combining the measured volatile concentrations in clinopyroxene (cpx) phenocrysts and apatite inclusions in phenocrysts with experimentally determined partition/exchange coefficients between minerals and melts (Callegaro et al., 2014; Meng et al., 2021). The advantages of this method are as follows: (1) Cpx and apatite are widely developed and crystallized early in the samples; (2) Apatite inclusions are not susceptible to volatile diffusion, crystallization or bubble growth after entrapment, and can effectively record the pre-eruptive volatile contents of magmas (Stock et al., 2016); and (3) The analytical methods of F, Cl and S in cpx and apatite are robust.

### 3.2.2 Electron microprobe analysis of S, Cl and F in apatite inclusions

Volatile compositions of apatite were determined with a Shimadzu electron probe microanalyzer (EMPA 1720H) at School of Earth Sciences, Zhejiang University. Backscattered electron images (BSE) were firstly used to check the homogeneity of minerals. 15 kV accelerating voltage, 10 nA beam current and 5  $\mu$ m beam size were set for analysis. Natural minerals and synthetic oxides were used as standards, and the final data correction was conducted by the ZAF program. The standard apatite (Durango; Van Hoose et al., 2013) was used to estimate the relative errors (1  $\sigma$ ) of F, Cl, and SO<sub>3</sub>, which were <13%, <10% and <15%, respectively. Moreover, we conducted map scanning (F, Cl and S) of representative apatite grains, operating with an accelerating voltage of 15 kV, a beam current of 10 nA, and a beam size of 1  $\mu$ m. The mineral compositions of cpx, biotite and amphibole were also determined, with the analytical conditions as follows: 15 kV accelerating voltage for all minerals, 20 nA beam current for cpx and 15 nA beam current for amphibole and biotite. The beam sizes were 5  $\mu$ m for cpx, and 1  $\mu$ m for amphibole and biotite. The errors of major elements were lower than 2%. The analyzed results of cpx, biotite and amphibole are described in the Supporting text.

### 3.2.3 Secondary ion mass spectroscopy (SIMS) analysis of S, Cl and F in cpx phenocrysts

After the EPMA analysis, the cpx grains were cleaned and mounted in indium targets. The mounts were made carefully to make sure that the analyzed spots by EPMA can be found for the following SIMS analysis. The samples were then polished and washed (by ethanol and acetone) to remove carbon coating and placed in a muffle furnace for 24 hours before gold coating. The concentrations of volatiles (F, Cl, S) in cpx phenocrysts were measured by a Cameca IMS-1270 instrument at CRPG-CNRS in Nancy, France. A primary Cs<sup>+</sup> beam of 0.26–1.08 nA was accelerated by a voltage of 10 kV to sputter the secondary ions with a diameter of 10  $\mu$ m. The sputtered secondary ions were extracted by a 10 kV voltage, and then counted by Faraday cups or electronic multipliers with a mass resolution of 7000. In each session, calibration slopes (m) were obtained by plotting measured the isotope ratios (x) of <sup>19</sup>F/<sup>30</sup>Si, <sup>35</sup>Cl/<sup>30</sup>Si and <sup>32</sup>S/<sup>30</sup>Si of the standard glasses against the known reference material concentrations (y), generating the equation  $y = mx$  (Fig. S1). The concentrations of F, Cl and S

in the unknown samples were then calculated by multiplying measured isotope ratios by  $m$ . The standard glasses are MQ47963 (776 ppm S, 777 ppm F and 1356 ppm Cl; Kamenetsky et al., 2000), VG2 (1424 ppm S, 300 ppm F and 298 ppm Cl; Jarosewich et al., 1980) and StHs (2.7 ppm S, 320 ppm F and 231 ppm Cl; Jochum et al., 2006). The relative average deviations of F, Cl and S obtained from the different standard samples were 7%, 4% and 2%, respectively.

### 3.2.4 Calculating S, Cl and F in the equilibrated melts

The partition coefficient of S between cpx and melt ( $D_s^{\text{cpx-m}}$ ) is critically affected by the melt composition (including water content), Mg# of cpx, and most importantly, oxygen fugacity (Callegaro et al., 2020). Previous works have obtained oxygen fugacities of basalts and HMAs representing the same strata as our samples indicate highly oxidized magmas with  $\Delta \log f_{\text{O}_2} \text{ FMQ} = +1.5 - +1.9$  and  $\Delta \log f_{\text{O}_2} \text{ FMQ} = +0.5 - +1.4$  (Hong et al., 2017; Geng et al., 2019). We thus use the partition coefficient formula of total S for the highly oxidized silicate melts:  $D_s^{\text{cpx-m}} = 0.003(\pm 0.002) \times (\text{SiO}_2) - 0.117(\pm 0.084)$  to calculate S in the equilibrated melts (Callegaro et al., 2020), where  $\text{SiO}_2$  is the content of bulk rock. The Cl partition coefficient between cpx and basaltic melt ( $D_{\text{Cl}}^{\text{cpx-m}}$ ) is affected by temperature, pressure, mineral composition and melt composition (including water content); the F partition coefficient between cpx and basaltic to dacitic melt ( $D_{\text{F}}^{\text{cpx-m}}$ ) is mainly controlled by mineral composition, melt water content and viscosity while the influences of temperature and pressure are limited (Dalou et al., 2012, 2014; Baker et al., 2022). According to the major-element compositions and crystallization conditions (1120–1240 °C and ~0.7 GPa) of cpx phenocrysts and the water contents of bulk rocks ( $3.7 \pm 2.1$  wt.% to  $4.3 \pm 1.3$  wt.%) (Geng et al., 2019), we chose the appropriate  $D_{\text{Cl}}^{\text{cpx-m}}$  and calculated  $D_{\text{F}}^{\text{cpx-m}}$  by using the empirical equation of  $\ln(D_{\text{F}}^{\text{cpx-m}}) = 0.2298(T/\text{NBO}) - 1.029(\text{Al}^{\text{M1}}) - 3889(1/T) - 0.5472(P) + 0.5871$  (see details in Table S2; Dalou et al., 2012, 2014; Baker et al., 2022). We then used the functions of  $S_{\text{melt}} (\text{wt.}\%) = S_{\text{cpx}} / D_s^{\text{cpx-m}}$ ,  $\text{Cl}_{\text{melt}} (\text{wt.}\%) = \text{Cl}_{\text{cpx}} / D_{\text{Cl}}^{\text{cpx-m}}$  and  $\text{F}_{\text{melt}} (\text{wt.}\%) = \text{F}_{\text{cpx}} / D_{\text{F}}^{\text{cpx-m}}$  to calculate the volatile contents in the equilibrated melts. The total uncertainties related to the applied methods are approximately <40% for the melt S content and ~20–26% for the melt Cl and F contents.

Additionally, we estimated volatile contents of melts that were in equilibrium with apatite inclusions. The factors affecting the S partition coefficient between apatite and melt ( $D_s^{\text{ap-m}}$ ) are complicated, mainly including the temperature, oxygen fugacity and S content of the melt (Parat et al., 2011; Webster & Piccoli, 2015; Konecke et al., 2019). We used the formula  $S_{\text{ap}} (\text{wt.}\%) = D_s^{\text{ap-m}}(f_{\text{O}_2}) \times S_{\text{melt}} \times [D_s^{\text{ap-m}}(\text{AST})/D_s^{\text{ap-m}}(1000^\circ\text{C})]$  (Meng et al., 2021) to calculate melt S contents, in which  $D_s^{\text{ap-m}}(f_{\text{O}_2})$ ,  $D_s^{\text{ap-m}}(\text{AST})$  and  $D_s^{\text{ap-m}}(1000^\circ\text{C})$  can be acquired from experimental data of Konecke et al. (2019) and Parat and Holtz (2004). This method was chosen because it considered the effects of both temperature and oxygen fugacity, and deviations between the measured and calculated results are limited

(Meng et al., 2021). Because of the non-Nernstian partitioning behavior of F and Cl between apatite and melt (Boyce et al., 2014), we used the exchange coefficients of F, Cl and OH between apatite and melt to quantify the volatile contents in the equilibrated melts. As proposed by Li and Hermann (2017), the empirical formulas of melt Cl and F contents under a felsic magmatic system are  $\text{Cl}_{\text{melt}}(\text{wt. \%}) = \frac{X_{\text{Cl}}^{\text{ap}}}{X_{\text{OH}}^{\text{ap}}} \frac{1}{\text{Kd}_{\text{Cl-OH}}^{\text{ap-melt}}} \times 10.79$ ,  $\text{Kd}_{\text{Cl-OH}}^{\text{ap-melt}} = e^{(25.81 + (X_{\text{Cl}}^{\text{ap}} - X_{\text{OH}}^{\text{ap}}) \times 17.33) \times \frac{10^3}{8.314 \times T}}$  and  $\text{F}_{\text{melt}}(\text{wt. \%}) = \frac{X_{\text{F}}^{\text{ap}}}{X_{\text{OH}}^{\text{ap}}} \frac{1}{\text{Kd}_{\text{F-OH}}^{\text{ap-melt}}} \times 6.18$ ,  $\text{Kd}_{\text{F-OH}}^{\text{ap-melt}} = e^{(40.33 + (X_{\text{F}}^{\text{ap}} - X_{\text{OH}}^{\text{ap}}) \times 21.29 - 3.96 \times X_{\text{Cl}}^{\text{ap}}) \times \frac{10^3}{8.314 \times T}}$ . The empirical formula for the melt Cl content in a basaltic magmatic system is  $\text{Cl}_{\text{melt}}(\text{wt. \%}) = \frac{X_{\text{Cl}}^{\text{ap}}}{X_{\text{OH}}^{\text{ap}}} \frac{1}{\text{Kd}_{\text{Cl-OH}}^{\text{ap-melt}}} \times 9.12$ , where  $\text{Kd}_{\text{Cl-OH}}^{\text{ap-melt}}$  is the same as that in a felsic magmatic system (Li & Hermann, 2017). The total uncertainties are approximately <40% for the calculated S content and ~20–33% for the calculated Cl content in the basaltic and felsic melts, while the total uncertainty of the calculated F content in the felsic melt is higher, up to ~55%.

## 4 Results

### 4.1 Bulk-rock major elements

In the total alkali vs.  $\text{SiO}_2$  diagram of Le Bas et al. (1986), the samples plot in the fields of rhyolite, trachydacite, trachyandesite and basalt (Fig. S2).

The rhyolites of the Zhangjiakou Formation (corresponding to Stage I) have high  $\text{SiO}_2$  of 69.24–72.06 wt.%, and low  $\text{TFe}_2\text{O}_3$  of 3.32–3.94 wt.%,  $\text{MgO}$  of 0.28–0.89 wt.% and  $\text{P}_2\text{O}_5$  of 0.17–0.23 wt.% (Fig. S3). In Stage II, the basalts of the Lower Yixian Formation are characterized by high  $\text{MgO}$  of 9.96–14.4 wt.%,  $\text{TFe}_2\text{O}_3$  of 8.81–9.85 wt.%,  $\text{P}_2\text{O}_5$  of 0.65–0.84 wt.% and  $\text{Mg\#}$  of 68.9–75.3 (Fig. S3; Table S1). Among them, the basalts from the Yixian County have obviously higher  $\text{MgO}$  and  $\text{TFe}_2\text{O}_3$  and lower  $\text{K}_2\text{O}$  and  $\text{P}_2\text{O}_5$  than those from the Sihetun County, and they belong to high-K calc-alkaline series and shoshonites series, respectively (Fig. S3-F). The trachyandesites of the Lower Yixian Formation are referred to as HMAs with unusually high  $\text{MgO}$  (>5 wt.%) and/or high  $\text{Mg\#}$  (>50) (Fig. S3-C; Tatsumi, 2008; Kelemen et al., 2014). They have significantly lower  $\text{P}_2\text{O}_5$  (0.48–0.50 wt.%),  $\text{TFe}_2\text{O}_3$  (6.93–7.11 wt.%) and  $\text{MgO}$  (5.60–6.22 wt.%) than basalts, yet higher than rhyolites in Stage I (Fig. S3). The trachydacite sample of the Upper Yixian Formation, which represents Stage III, has  $\text{SiO}_2$  of 68.14 wt.%,  $\text{TFe}_2\text{O}_3$  of 4.00 wt.%,  $\text{MgO}$  of 0.87 wt.% and  $\text{P}_2\text{O}_5$  of 0.23 wt.% (Fig. S3), which are nearly comparable with those measured for rhyolites in Stage I.

### 4.2 Volatile (S, Cl, F) contents of clinopyroxene phenocrysts and apatite inclusions

Clinopyroxene phenocrysts only occur in basalts and HMAs of the Lower Yixian Formation (corresponding to Stage II) and are compositionally augite and diopside. Compared with cpx in basalts from the Yixian County, which display

F and Cl contents of 103.2–438.3 ppm and 1.5–61.7 ppm (mostly <30 ppm), respectively, the cpx grains in HMAs have slightly lower F (43.1–314.4 ppm) and Cl (2.5–23.9 ppm), while those in basalts from the Sihetun County show much lower F of 58.3–94.7 ppm and Cl of 2.1–12.8 ppm (Table S2; Figs. 3A and 3B). Sulphur contents of all cpx phenocrysts are similar: 0.9–10.7 ppm for basalts from the Yixian County, 2.1–6.5 ppm for HMAs, and 2.1–18.4 ppm for basalts from the Sihetun County (Fig. 3C).

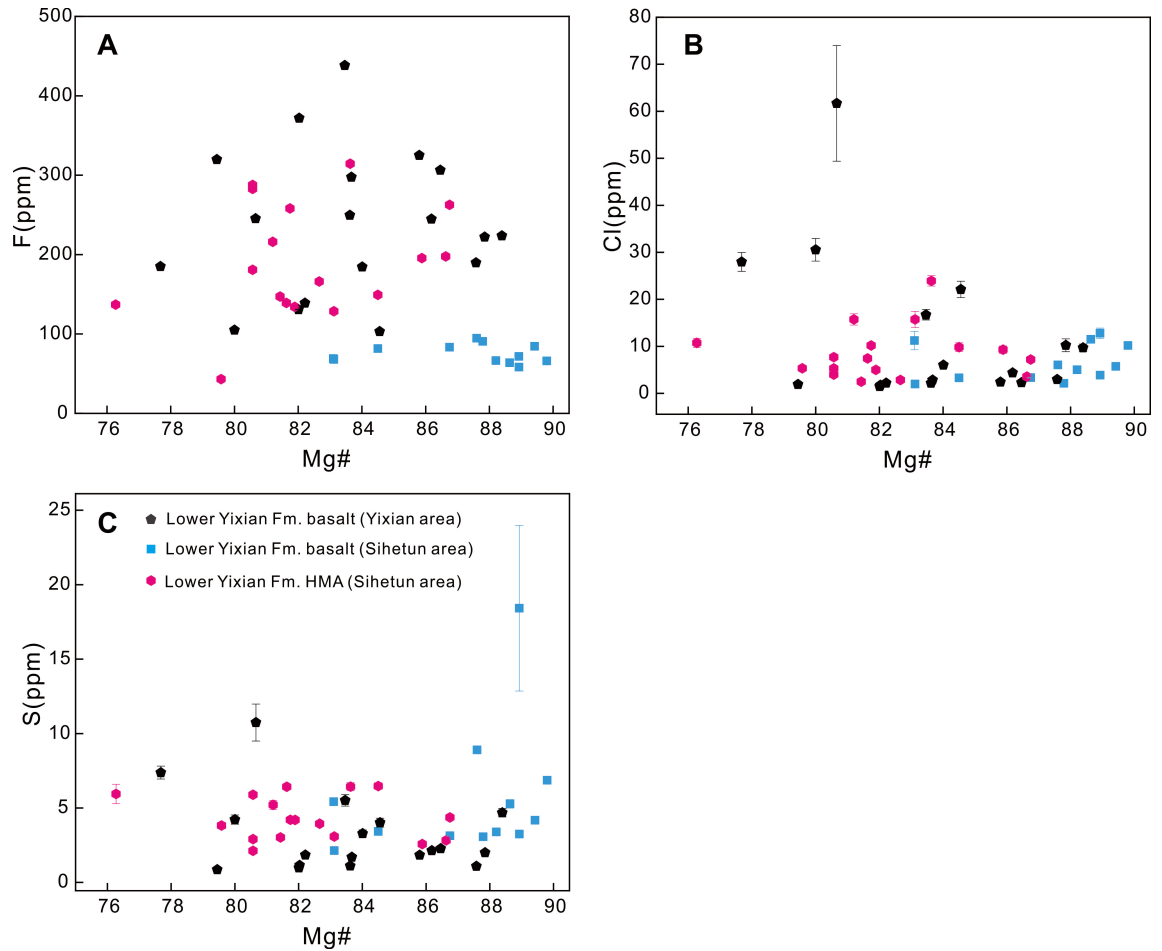


**Figure 3.** F (A), Cl (B), and S (C) contents versus Mg# of clinopyroxene in basalts and high-Mg andesites (HMAs) of the Lower Yixian Formation.

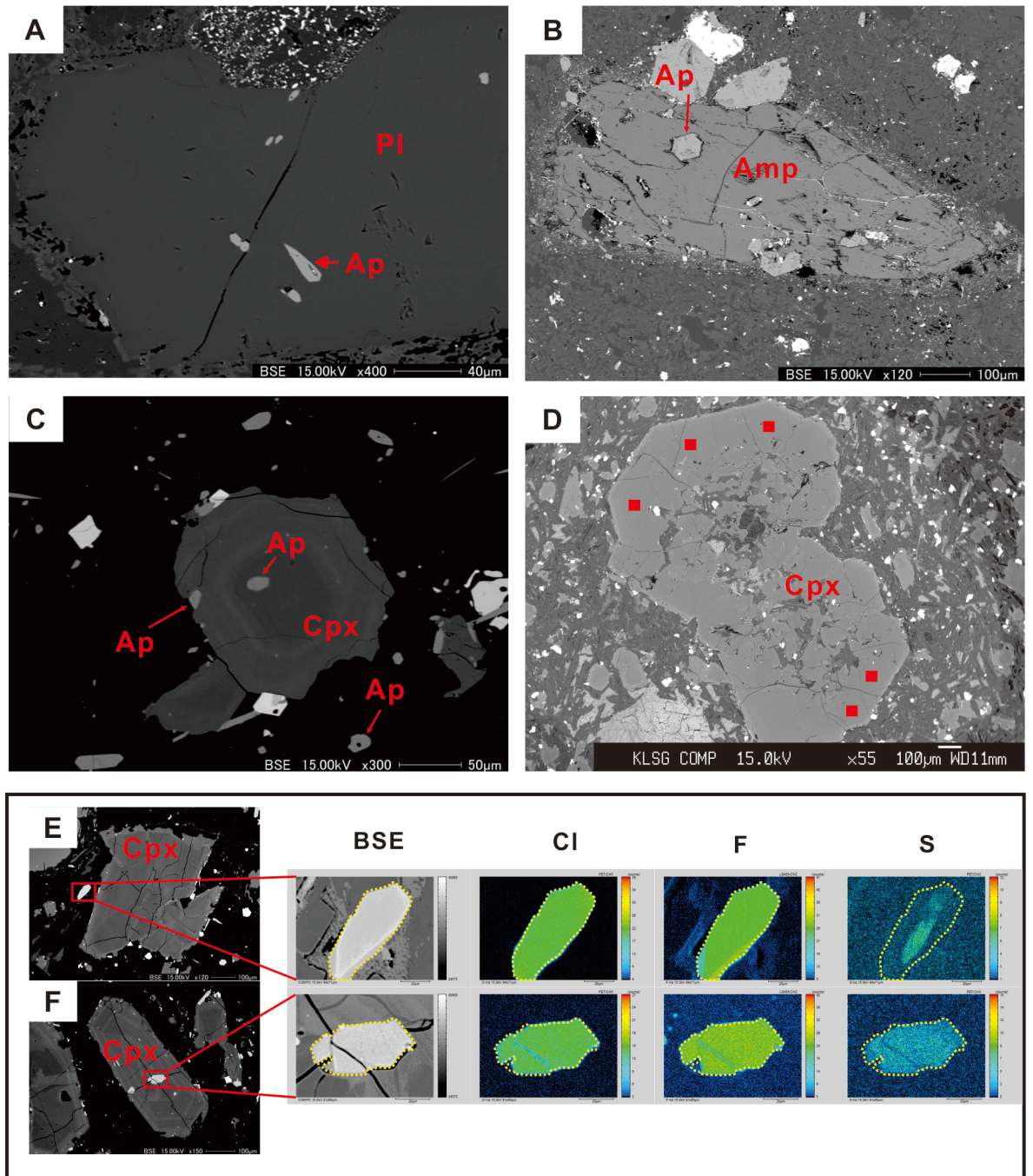


**Figure 4.** BSE images of studied volcanic rocks from the Zhangjiakou (A-B) and Yixian Formations (C-D). BSE images and Cl, F and S maps of a repre-

sentative apatite microphenocryst (E) and inclusion (F) in studied samples. Pl-plagioclase; Ap-apatite; Amp-amphibole; Cpx-clinopyroxene. The red squares show the analytical points of SIMS.

Apatite crystals are well developed in all samples, occurring either as microphenocrysts associated with other phenocrysts, or as euhedral inclusions in coarser phenocrysts (Fig. 4). Apatite microphenocrysts show heterogeneous compositions indicating possible diffusional modification (Fig. 4E), while apatite inclusions are usually homogeneous (Fig. 4F). We focused on those apatite crystals that are included in early-crystallized phenocrysts (Fig. 4), such as plagioclase and amphibole phenocrysts in rhyolites (Stage I), cpx phenocrysts in basalts and HMAs (Stage II), and biotite and plagioclase phenocrysts in the trachydacite sample (Stage III). They are mainly fluorapatites and minor hydroxyapatites and mostly show a volcanic origin (Table S3; Fig. S4). In rhyolites of Stage I, they have high Cl contents of 0.003–1.37 wt.% and  $\text{SO}_3$  of 0.17–0.88 wt.%. By contrast, the apatite inclusions in Stage II basalts and HMAs show lower Cl (0.04–0.70 and 0.13–0.40 wt.%) and  $\text{SO}_3$  (0.01–0.63 wt.% and 0.26–0.84 wt.%) contents. In particular, apatite inclusions in basalts from the Sihetun County contain the lowest Cl (0.04–0.16 wt.%) and  $\text{SO}_3$  (0.25–0.46 wt.%) contents among all the samples (Fig. 5A). Stage III is represented by trachydacite with Cl of 0.61–1.56 wt.% and  $\text{SO}_3$  of 0.17–1.22 wt.% in apatite inclusions, which are comparable or higher than those of rhyolites in Stage I (Fig. 5A). Fluorine contents of apatite inclusions display little differences between the samples, ranging from 1.10 to 3.43 wt.% (Fig. 5B).

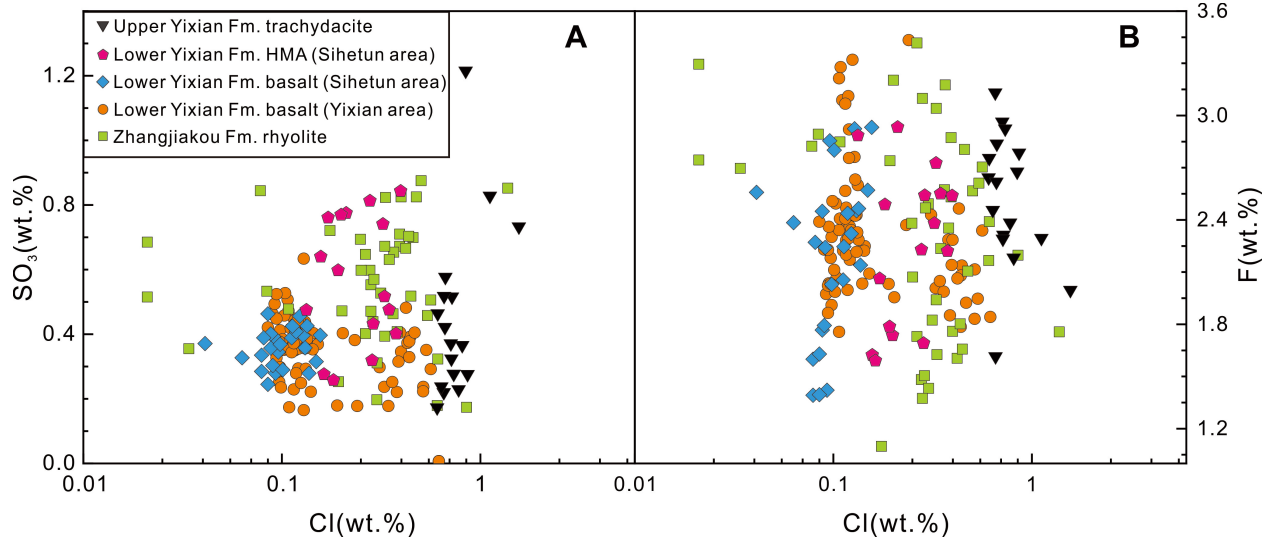


**Figure 5.** Plots of  $\text{SO}_3$  (A) and F (B) vs. Cl contents for apatite inclusions in the studied samples from the Zhangjiakou and Yixian Formations.

#### 4.3 Pre-eruptive magmatic volatile (F, Cl and S) contents

### 4.3.1 Sulfur

The calculated S contents of melts in equilibrium with cpx are 17–632 ppm, 43–1083 ppm, and 24–259 ppm for Yixian basalts, Sihetun basalts and HMAs in Stage II, respectively (Table S2; Fig. 6A). The obtained melt S contents in equilibrium with apatite are 566–3288 ppm for rhyolites (Stage I), 16–1422 ppm for Yixian basalts (Stage II), 452–914 ppm for Sihetun basalts (Stage II), 765–2370 ppm for HMAs (Stage II), and 283–1991 ppm for trachydacite (Stage III), respectively (Table S3; Fig. 6A). The calculation details are given in the Supporting text. It is noteworthy that although Callegaro et al. (2020) suggested to use synchrotron X-ray microfluorescence to measure the low S concentration in cpx, our results show similar independent results calculated from the apatite- and cpx-based methods within one order of magnitude (Fig. 6A). It is noteworthy that although Callegaro et al. (2020) suggested to use synchrotron X-ray microfluorescence to measure the low S concentration in cpx, our results show similar independent results calculated from the apatite- and cpx-based methods within one order of magnitude (Fig. 6A).

### 4.3.2 Chlorine and Fluorine

By combining the Cl and F contents of cpx phenocrysts and the partition coefficients for Cl and F between cpx and basaltic to andesitic melt, we obtained Cl of 99–5608 ppm and F of 753–3746 ppm for basalts from the Yixian County (Stage II), relatively lower Cl of 132–1162 ppm and F of 439–891 ppm for basalts from the Sihetun County (Stage II), and Cl of 62–1710 ppm and F of 295–2707 ppm in HMAs (Stage II) (Table S2; Figs. 6B and 6C). The calculated Cl and F contents of melts in equilibrium with apatite show that the rhyolites (Stage I) have Cl of 26–7915 ppm and F of 982–3132 ppm, the Yixian and Sihetun basalts and HMAs (Stage II) have Cl of 409–2747 ppm, 221–1277 ppm and 728–2182 ppm, and the trachydacite (Stage III) has Cl of 3410–12315 ppm and F of 1051–2450 ppm (Table S3; Figs. 6B and 6C). As shown in Fig. 6B, the cpx- and apatite-based melt Cl abundance estimates are nearly comparable.

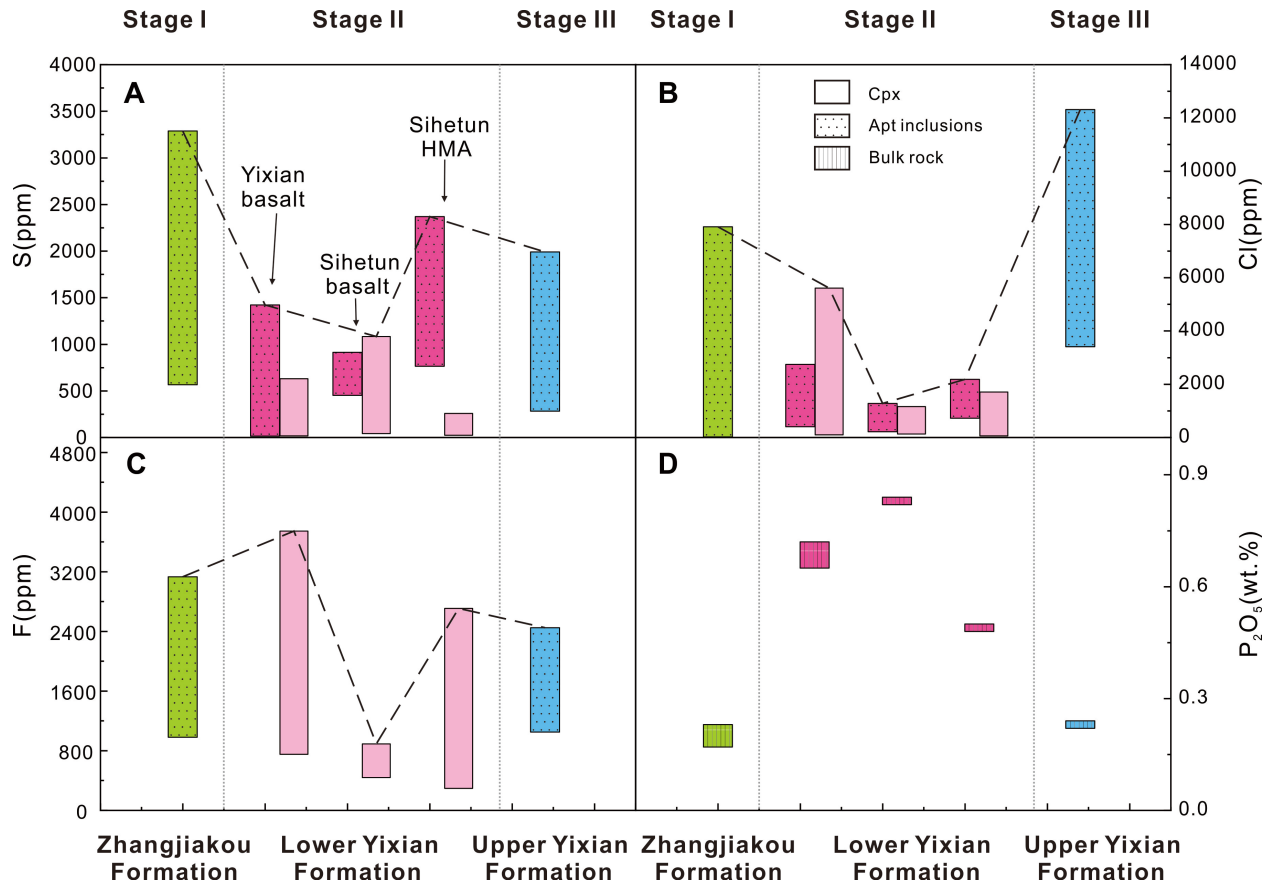


**Figure 6.** Volatile (S, Cl, F) and P<sub>2</sub>O<sub>5</sub> contents of the studied volcanic rocks around Stage I (pre-flourishing), Stage II (flourishing) and Stage III (post-flourishing) of the Jehol Biota. The dashed lines mark the maximum values that were used to represent the pre-eruptive magmatic volatile contents of our samples.

## 5 Discussion

### 5.1 Effects of volcanic gases

The wide range of F, Cl and S contents in most clinopyroxene phenocrysts and apatite inclusions may be related to complex magmatic evolution processes, such as fractional crystallization and syn-eruptive degassing (Figs. 3 and 5). Given potential degassing prior to clinopyroxene and apatite crystallization (Callegaro et al., 2014), we interpret the maximum S, Cl and F concentrations to be most representative of the pre-eruptive magmatic volatile contents. Most volcanic samples corresponding to Stage I and Stage III show higher S (3288 ppm and 1991 ppm) and Cl (7915 ppm and 12315 ppm) contents than volcanic samples corresponding to Stage II with S of 1083–2370 ppm and Cl of 1277–5608 ppm

(Figs. 7A-B). There is no obvious difference in the F contents, which range from 893 to 3746 ppm, between the different stages (Fig. 7C).

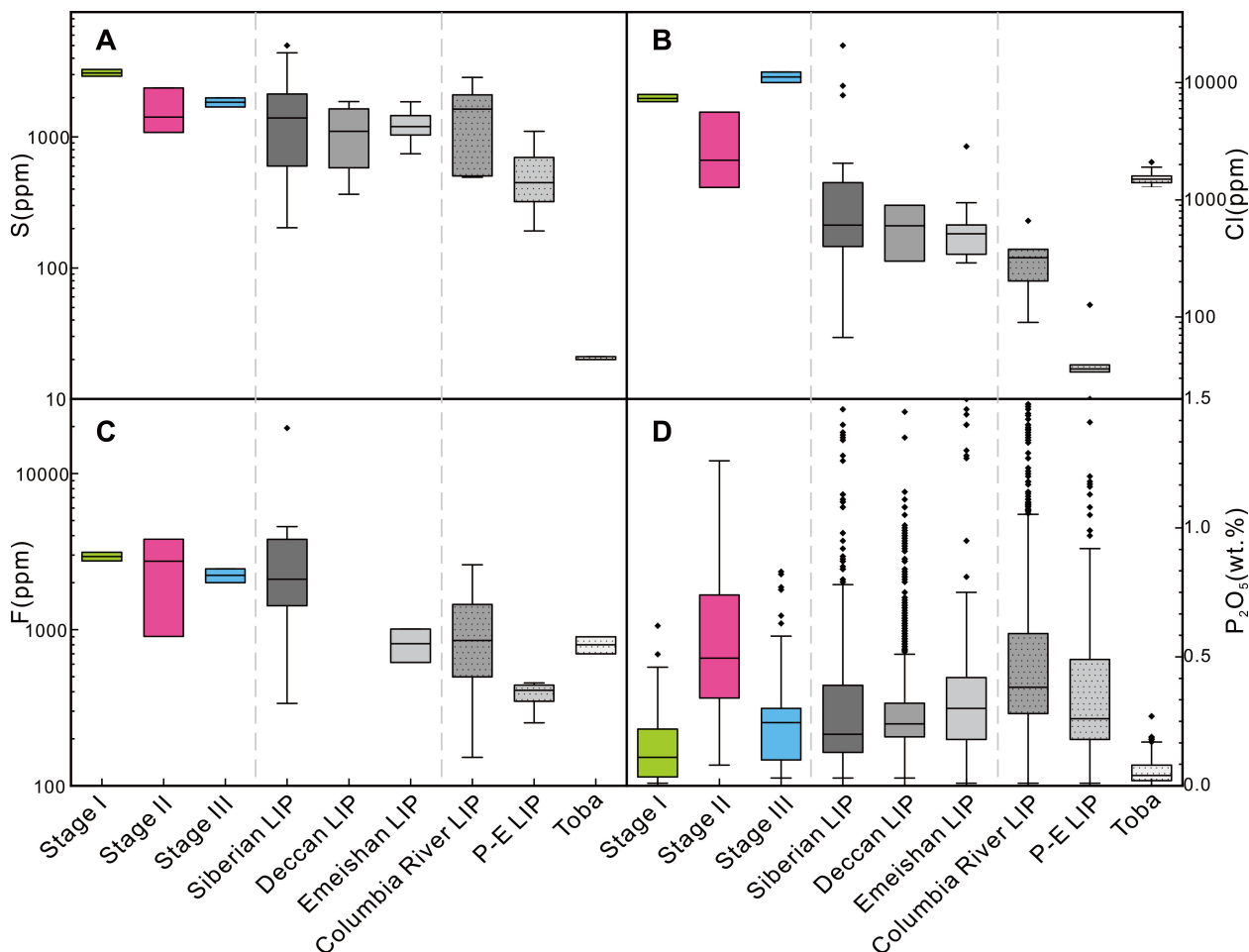


**Figure 7.** S (A), Cl (B), F (C) and  $P_2O_5$  (D) contents of the studied samples around Stage I (pre-flourishing), Stage II (flourishing) and Stage III (post-flourishing) of the Jehol Biota, as well as other volcanic events including typical large igneous provinces (LIPs) and Toba volcano. Data sources are given in Table S5.

A ‘petrological method’ was used to calculate the total masses of volatiles released in volcanic activities (see calculation details and results in the Supporting text and Table S4). By using the estimated volumes ( $10^2$  to  $10^5$  km<sup>3</sup>) of the lava flows in different stages, the total masses of released S, Cl and F are estimated to be respectively 34–690 Gt, 47–934 Gt and 15–308 Gt in Stage I (duration of ca. 10 Ma); 3.6–6.6 Gt, 2.2–4.6 Gt and 2.1–4.0 Gt in Stage II (duration of <0.3 Ma); and 1–29 Gt, 4–102 Gt and 1–17 Gt in Stage III (duration of <1

Ma). These data clearly show that the volcanic activity in Stage II produced the lowest total emissions (Fig. 8) and/or average fluxes of S, Cl and F. To evaluate the climatic and environmental effects of volcanic gases, we compiled the S, Cl and F contents and total masses of five LIPs associated both with devastating (Siberia, Deccan and Emeishan LIPs) and negligible (Columbia River and Paraná-Etendeka LIPs) environmental and biotic impacts (Ernst & Youbi, 2017; Clapham & Renne, 2019), as well as Toba, the largest volcanic eruption (ca. 75ky with volumes of 2500 3000 km<sup>3</sup>; Chesner et al., 1991) since the Pleistocene with limited impacts (Louys, 2007; Timmreck et al., 2012; Lane et al., 2013) (Table S5). Our data show that the Stage II volcanism has elevated S, F and Cl concentrations that are equivalent to or higher than those of LIPs associated with devastating environmental impacts and mass extinctions (Fig. 7). However, the average fluxes of S, Cl and F of Stage II are much lower than those in all LIPs due to the limited total S, Cl and F emissions that are similar to those of Toba (Fig. 8). The result indicates insignificant climatic and environmental impacts induced by volcanic emissions in Stage II. The prevalently warm and humid climate in Stage II with short and seasonal intervals of cold and drought (Yang et al., 2013; Zhou, 2014) are more likely controlled by the fluctuating global climate in the Early Cretaceous (Price & Hart, 2002; Keller, 2008). In contrast, the volcanic eruptions in Stage I and Stage III show both elevated concentrations and total emissions of S, Cl and F, with the emissions being higher than those of Toba by 1 3 orders of magnitude (Fig. 8). In particular, the upper levels of the total volatile emissions in Stage I can reach the amounts of the Deccan or Emeishan LIPs (Fig. 8). However, the average volatile fluxes of Stages I and III are lower than those in all LIPs, indicating minor global impacts. Thus we conclude that the prolonged volcanic eruptions may have catastrophic effects on the local environment in Stages I and III, including episodic acid rain, poisoning of the ecosystem (by fluorine and trace metals), vegetation damage (shedding of leaves, charring and decreasing the stomatal density), enhanced soil erosion (by strong rainfall and acidification), and possibly enhanced nucleation of storm clouds and wildfires (Garrec et al., 1977; Le Guern et al., 1988; Binkley et al., 1989; Wilson et al., 2011; Haworth et al., 2012; Bacan et al., 2013).

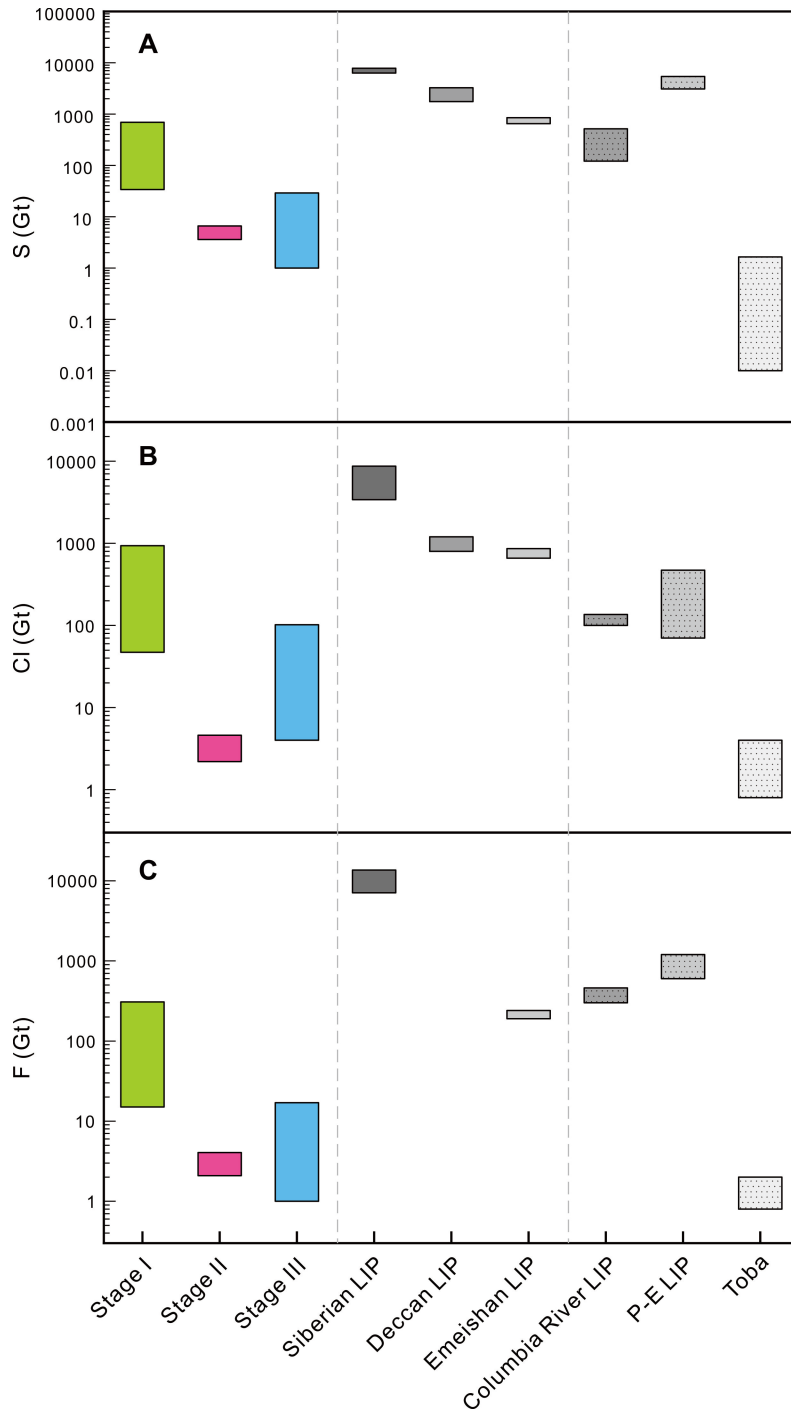


**Figure 8.** Total masses of released S (A), Cl (B) and F (C) of the early

Cretaceous volcanism in the eastern North China craton around Stage I (pre-flourishing), Stage II (flourishing) and Stage III (post-flourishing) of the Jehol Biota and other volcanic events. Data sources are given in Table S5.

### 5.2 Effects of phosphorus released from weathered volcanic rocks

In addition to the climatic and environmental effects via gas emissions (Mather, 2015), the lavas can release essential nutrients for life through weathering. Phosphorus is one of the most important limiting nutrients, providing a fundamental control on primary productivity (Tyrrell, 1999; Elser et al., 2007). Our results show that stage II is dominated by intermediate-mafic volcanic rocks with relatively higher  $P_2O_5$  contents (median 0.50 wt.%) compared to Stages I and III (median 0.11 wt.% and 0.24 wt.%), Toba (0.04 wt.%) and all LIPs (median 0.2–0.38 wt.%) (Fig. 7D and Table S5). Phosphorus limitation had been evidenced to be strongly influenced by the parental material, especially the bedrock geochemistry (Vitousek et al., 2010; Augusto et al., 2017). Moreover, in the NCC, the predominant Early Cretaceous warm and humid climate (Li & Battern, 2007; Yang et al., 2013), well-developed river systems (Liu et al., 2015) and acidified surface environment (Zhou et al., 2016) undoubtedly contributed to weathering of P-rich volcanic terrains and transporting P into the ecosystem. In addition to P, the possibly enhanced Fe flux sourced from the weathered intermediate-mafic lavas may play a subordinate role in promoting primary production (Martin et al., 1994). These may decipher the flourishing of charophytes (Wang et al., 2008), gold algae (Hethke et al., 2013), bacterium and aquatic plants (Li et al., 2016) and terrestrial vegetation (Wu, 2008) in Stage II, with fossil-bearing sediments showing high total organic carbon (TOC) values up to 5.56 wt.% (Zhang et al., 2016). In contrast, the P-depleted intermediate-felsic volcanic rocks in Stages I and III are mainly composed of quartz and K-feldspar, which are resistant to weathering. The lack of P input may be an important limiting factor for primary productivity in terrestrial ecosystems in those times.

### 5.3 Implications for terrestrial biota evolution

Our study demonstrates that the ecosystem deterioration related to poisonous gas emissions (F, Cl and S) and the limited availability of nutrient P hindered the survival and reproduction of species during the pre-flourishing (Stage I) and post-flourishing (Stage III) periods of the Jehol Biota. Instead, the climatic and environmental effects induced by volatile degassing were negligible in the flourishing Stage II. The enhanced volcanogenic P flux increased primary productivity and promoted the greatest species diversification and largest radiation of the Jehol Biota at that time.

Generally, the abundances of P in the upper silicate crust are low due to the accumulation of most P in the Earth's interior during early differentiation (Rudnick & Gao, 2014). Thus, the processes of mantle melting and magmatism are critical for recycling P (incompatible element) from the deep Earth to the surface (Horton, 2015). The increased P flux in the flourishing period is consistent with the intense eruption of intermediate-mafic lavas produced by melting of

lithospheric mantle during the peak destruction of the NCC. Therefore, we propose that the deep-Earth material cycle associated with the NCC destruction was probably the critical driving force for the flourishing of the Jehol Biota, providing sufficient amounts of limiting nutrients (e.g., P, Fe) for the surface ecological environment. The unique geodynamic process in the eastern NCC may have determined the greater species diversification of the Jehol Biota than that of contemporaneous Santana Biota in Brazil and Las Hoyas Biota in Spain characterized by similar freshwater ecosystems. Similar examples include: (1) The weathering of large-scale LIPs formed by the breakup of the Rodinia supercontinent resulted in extremely high P fluxes in the global oceans in the early and middle Neoproterozoic (Cox et al., 2016; Horton, 2015), which might have increased primary productivity and triggered ocean-atmosphere oxidation and life explosion during that period (Gernon et al., 2016); (2) The continuous increases of P contents of igneous rocks affected by long-term mantle cooling enhanced primary productivity and photosynthesis, and correlated with the rising atmospheric oxygen levels throughout geological history (Cox et al., 2018); and (3) The high TOC values of the Mesoproterozoic Kyalla Formation in Australia might be related to P enrichment in sedimentary basins caused by the weathering of Derim-Galiwinku LIP (Yang et al., 2020). Our study provides a unique case to reveal the coupling relationship between biosphere and deep geodynamic processes driven by volcanism at the local scale.

## 6 Conclusions

(1) The pre-eruptive magmatic S, Cl and F contents of the early Cretaceous volcanism in the eastern NCC are 3288 ppm, 7915 ppm and 3132 ppm in Stage I (the pre-flourishing period of the Jehol Biota); 1083–2370 ppm, 1277–5608 ppm and 893–3746 ppm in Stage II (the flourishing period of the Jehol Biota); and 1991 ppm, 12315 ppm and 2450 ppm in Stage III (the post-flourishing period of the Jehol Biota). The total emissions of S, Cl and F are 34–690 Gt, 47–934 Gt and 15–308 Gt in Stage I; 3.6–6.6 Gt, 2.2–4.6 Gt and 2.1–4.0 Gt in Stage II; and 1–29 Gt, 4–102 Gt and 1–17 Gt in Stage III.

(2) The total amounts of volatiles (S, Cl and F) released by volcanism during the flourishing period of the Jehol Biota were relatively low and had negligible impacts on local climate and environment. The large amounts of P input sourced from the weathering of intermediate-mafic volcanic rocks probably enhanced the primary productivity of the ecosystem, which might be the important factor to induce the flourishing of the Jehol Biota.

(3) Volcanic activity in the non-flourishing period of the Jehol Biota emitted relatively abundant toxic gases, which might cause the deterioration of the local climate and environment. Combined with the limited P sources (predominately felsic bedrocks), the living conditions in these two stages are unfavorable for the species diversification.

## Acknowledgments

We thank Can Rao and Su-Wen Qiu for their help with the EMPA analysis.

We are also grateful to Yu-Xin He and Kong-Yang Zhu for their discussion. This work was supported by the National Natural Science Foundation of China (Grant 41688103) and Fundamental Research Funds for the Central Universities (Grant K20210168).

### Data Availability Statement

Datasets for this research are available in Zenodo (<https://doi.org/10.5281/zenodo.6354942>).

### References

- Augusto, L., Achat, D. L., Jonard, M., Vidal, D., & Ringeval, B. (2017). Soil parent material—A major driver of plant nutrient limitations in terrestrial ecosystems. *Global Change Biology*, *23*, 3808–3824. <https://doi.org/10.1111/gcb.13691>
- Bacon, K. L., Belcher, C. M., Haworth, M., & McElwain, J. C. (2013). Increased atmospheric SO<sub>2</sub> detected from changes in leaf physiognomy across the Triassic–Jurassic boundary interval of East Greenland. *PLoS ONE*, *8*(4), e60614. doi: 10.1371/journal.pone.0060614
- Baker, D. R., Callegaro, S., De Min, A., Whitehouse, M. J., & Marzoli, A. (2022). Fluorine partitioning between quadrilateral clinopyroxenes and melt. *American Mineralogist*, *107*, 167–177. <https://doi.org/10.2138/am-2021-7868>
- Binkley, D., Driscoll, C. T., Allen, H. L., Schoeneberger, P., & McAvoy, D. (1989). Acidic deposition and Forest Soil. Springer-Verag, New York. p. 149.
- Boyce, J. W., Tomlinson, S. M., McCubbin, F. M., Greenwood, J. P., & Treiman, A. H. (2014). The Lunar Apatite Paradox. *Science*, *344*, 400–402. doi: 10.1126/science.1250398
- Callegaro, S., Baker, D. R., De Min, A., Marzoli, A., Geraki, K., Bertrand, H., Viti, C., & Nestola, F. (2014). Microanalyses link sulfur from large igneous provinces and Mesozoic mass extinctions. *Geology*, *42*, 895–898. <https://doi.org/10.1130/G35983.1>
- Callegaro, S., Geraki, K., Marzoli, A., De Min, A., Maneta, V., & Baker, D. R. (2020). The quintet completed: The partitioning of sulfur between nominally volatile-free minerals and silicate melts. *American Mineralogist* *105*, 697–707. <https://doi.org/10.2138/am-2020-7188>
- Chesner, C. A., Rose, W. L., Drake, A. D. R., & Westgate, J. A. (1991). Eruptive history of Earth's largest Quaternary caldera (Toba, Indonesia) clarified. *Geology*, *19*, 200–203. [https://doi.org/10.1130/0091-7613\(1991\)019<0200:EHOESL>2.3.CO;2](https://doi.org/10.1130/0091-7613(1991)019<0200:EHOESL>2.3.CO;2)
- Clapham, M. E., & Renne, P. R. (2019). Flood Basalts and Mass Extinctions. *Annual Review of Earth and Planetary Sciences*, *47*, 275–303. <https://doi.org/10.1146/annurev-earth-053018-060136>
- Cox, G. M., Halverson, G. P., Stevenson, R. K., Vokaty, M., Poirier, A., Kunzmann, M., Li, Z. X., Denyszyn, S. W., Strauss, J. V., & Macdonald,

- F. A. (2016). Continental flood basalt weathering as a trigger for Neoproterozoic Snowball Earth. *Earth and Planetary Science Letters*, *446*, 89–99. <https://doi.org/10.1016/j.epsl.2016.04.016>
- Cox, G. M., Lyons, T. W., Mitchell, R. N., Hasterok, D., & Gard, M. (2018). Linking the rise of atmospheric oxygen to growth in the continental phosphorus inventory. *Earth and Planetary Science Letters*, *489*, 28–36. <https://doi.org/10.1016/j.epsl.2018.02.016>
- Dalou, C., Koga, K. T., Le Voyer, M., & Shimizu, N. (2014). Contrasting partition behavior of F and Cl during hydrous mantle melting implications for Cl/F signature in arc magmas. *Progress in Earth and Planetary Science*, *1*, 26. <https://doi.org/10.1186/s40645-014-0026-1>
- Dalou, C., Koga, K. T., Shimizu, N., Boulon, J., & Devidal, J. L. (2012). Experimental determination of F and Cl partitioning between lherzolite and basaltic melt. *Contributions to Mineralogy and Petrology*, *163*, 591–609. <https://doi.org/10.1007/s00410-011-0688-2>
- Elser, J. J., Bracken, M. E. S., Cleland, E. E., Gruner, D. S., Harpole, W. S., Hillebrand, H., Ngai, J. T., Seabloom, E. W., Shurin, J. B., & Smith, J. E. (2007). Global analysis of nitrogen and phosphorus limitation of primary producers in freshwater, marine and terrestrial ecosystems. *Ecology Letters*, *10*, 1135–1142. <https://doi.org/10.1111/j.1461-0248.2007.01113.x>
- Ernst, R. E., & Youbi, N. (2017). How Large Igneous Provinces affect global climate, sometimes cause mass extinctions, and represent natural markers in the geological record. *Palaeogeography, Palaeoclimatology, Palaeoecology*, *478*, 30–52. <https://doi.org/10.1016/j.palaeo.2017.03.014>
- Garrec, J. P., Lounowski, A., & Plebin, R. (1977). The influence of volcanic fluoride emissions on the surrounding vegetation. *Fluoride*, *10*(4), 152–156.
- Geng, X. L., Foley, S. F., Liu, Y. S., Wang, Z. C., Hu, Z. C., & Zhou, L. (2019). Thermal-chemical conditions of the North China Mesozoic lithospheric mantle and implication for the lithospheric thinning of cratons. *Earth and Planetary Science Letters*, *516*, 1–11. <https://doi.org/10.1016/j.epsl.2019.03.012>
- Gernon, T. M., Hincks, T. K., Tyrrell, T., Rohling, E. J., & Palmer, M. R. (2016). Snowball Earth ocean chemistry driven by extensive ridge volcanism during Rodinia breakup. *Nature Geoscience*, *9*, 242–248. <https://doi.org/10.1038/ngeo2632>
- Haworth, M., Elliott-Kingston, C., Gallagher, A., Fitzgerald, A., & McElwain, J. C. (2012). Sulphur dioxide fumigation effects on stomatal density and index of non-resistant plants: Implications for the stomatal palaeo-[CO<sub>2</sub>] proxy method. *Review of Palaeobotany and Palynology*, *182*, 44–54. <https://doi.org/10.1016/j.revpalbo.2012.06.006>
- Hethke, M., Fürsich, F. T., Jiang, B. Y., & Klaus, R. (2013). Oxygen deficiency in Lake Sihetun; formation of the Lower Cretaceous Liaoning Fossil-

lagerstätte (China). *Journal of the Geological Society, London* 170, 817–831. <https://doi.org/10.1144/jgs2012-102>

Hong, L. B., Zhang, Y. H., Xu, Y. G., Ren, Z. Y., Yan, W., Ma, Q., Ma, L., & Xie, W. (2017). Hydrous orthopyroxene-rich pyroxenite source of the Xinkailing high magnesium andesites, Western Liaoning: Implications for the subduction-modified lithospheric mantle and the destruction mechanism of the North China Craton. *Lithos*, 282–283, 10–22. <https://doi.org/10.1016/j.lithos.2017.02.014>

Horton, F. (2015). Did phosphorus derived from the weathering of large igneous provinces fertilize the Neoproterozoic ocean? *Geochemistry, Geophysics, Geosystems*, 16, 1723–1738. <https://doi.org/10.1002/2015GC005792>

Jarosewich, E., Nelen, J. A., & Norberg, J. A. (1980). Reference samples for electron microprobe analysis. *Geostandards Newsletter*, 4(1), 43–47. <https://doi.org/10.1111/j.1751-908X.1980.tb00273.x>

Jiang, B. Y., Harlow, G. E., Wohletz, K., Zhou, Z. H., & Meng, J. (2014). New evidence suggests pyroclastic flows are responsible for the remarkable preservation of the Jehol biota. *Nature Communications*, 5, 3151. <https://doi.org/10.1038/ncomms4151>

Jochum, K. P., Stoll, B., Herwig, K., Willbold, M., Hofmann, A. W., Amini, M., Aarburg, S., Abouchami, W., Hellebrand, E., Mocek, B., Raczek, I., Stracke, A., Alard, O., Bouman, C., Becker, S., Dücking, M., Brätz, H., Klemm, R., de Bruin, D., Canil, D., Cornell, D., de Hoog, C. J., Dalpé, C., Danyushevsky, L., Eisenhauer, A., Gao, Y. J., Snow, J. E., Groschopf, N., Günther, D., Latkoczy, C., Guillaumont, M., Hauri, E. H., Höfer, H. E., Lahaye, Y., Horz, K., Jacob, D. E., Kasemann, S. A., Kent, A. J. R., Ludwig, T., Zack, T., Mason, P. R. D., Meixner, A., Rosner, M., Misawa, K., Nash, B. P., Pfänder, J., Premo, W. R., Sun, W. D., Tiepolo, M., Vannucci, R., Vennemann, T., Wayne, D., & Woodhead, J. D. (2006). MPI-DING reference glasses for in situ microanalysis: New reference values for element concentrations and isotope ratios. *Geochemistry, Geophysics, Geosystems*, 7, Q02008. <https://doi.org/10.1029/2005GC001060>

Kamenetsky, V. S., Everard, J. L., Crawford, A. J., Varne, R., Eggins, S. M., & Lanyon, R. (2000). Enriched End-member of Primitive MORB Melts: Petrology and Geochemistry of Glasses from Macquarie Island (SW Pacific). *Journal of Petrology*, 41, 411–430. <https://doi.org/10.1093/petrology/41.3.411>

Kelemen, P. B., Hanghøj, K., & Greene, A. R. (2014). One View of the Geochemistry of Subduction-Related Magmatic Arcs, with an Emphasis on Primitive Andesite and Lower Crust. In Rudnick, R. L. (ed), *Treatise on Geochemistry, second ed.* (pp. 749–806). New York: Elsevier. <https://doi.org/10.1016/B978-0-08-095975-7.00323-5>

Keller, G. (2008). Cretaceous climate, volcanism, impacts, and biotic effects. *Cretaceous Research*, 29, 754–771. <https://doi.org/10.1016/j.cretres.2008.05.030>

Konecke, B. A., Fiege, A., Simon, A. C., Linsler, S., & Holtz, F.

(2019). An experimental calibration of a sulfur-in-apatite oxybarometer for mafic systems. *Geochimica et Cosmochimica Acta*, 265, 242–258. <https://doi.org/10.1016/j.gca.2019.08.044>

Lane, C. S., Chorn, B. T., & Johnson, T. C. (2013). Ash from the Toba supereruption in Lake Malawi shows no volcanic winter in East Africa at 75 ka. *Proceedings of the National Academy of Sciences of the United States of America*, 110, 8025–8029. <https://doi.org/10.1073/pnas.1301474110>

Le Bas, M. J., Le Maitre, R. W., Streckeisen, A., & Zanettin, B. (1986). A Chemical Classification of Volcanic Rocks Based on the Total Alkali–Silica Diagram. *Journal of Petrology*, 27, 745–750. <https://doi.org/10.1093/petrology/27.3.745>

Le Guern, F., Faivre-Pierret, H., & Garrec, J. P. (1988). Atmospheric contribution of volcanic sulphur vapour and its influence on the surrounding vegetation. *Journal of Volcanology and Geothermal Research*, 35, 173–178. [https://doi.org/10.1016/0377-0273\(88\)90014-5](https://doi.org/10.1016/0377-0273(88)90014-5)

Li, H.J., & Hermann, J. (2017). Chlorine and fluorine partitioning between apatite and sediment melt at 2.5 GPa, 800 °C: A new experimentally derived thermodynamic model. *American Mineralogist*, 102, 580–594. <https://doi.org/10.2138/am-2017-5891>

Li, J. G., & Batten, D. J. (2007). Palynological evidence of an Early Cretaceous age for the Yixian Formation at Sihetun, western Liaoning, China. *Cretaceous Research*, 28, 333–338. <https://doi.org/10.1016/j.cretres.2006.07.009>

Li, Y., Song, Z. G., Cao, X. X., & George, S. C. (2016). Sedimentary organic matter record of Early Cretaceous environmental changes in western Liaoning Province, NE China. *Organic Geochemistry*, 98, 54–65. <https://doi.org/10.1016/j.orggeochem.2016.05.010>

Liu, D.Y., Nutman, A. P., Compston, W., Wu, J. S., & Shen, Q. H. (1992). Remnants of 3800 Ma crust in the Chinese part of Sino-Korean craton. *Geology*, 20, 339–342. [https://doi.org/10.1130/0091-7613\(1992\)020<0339:ROMCIT>2.3.CO](https://doi.org/10.1130/0091-7613(1992)020<0339:ROMCIT>2.3.CO)

2

Liu, J., Xia, Q. K., Deloule, E., Ingrin, J., Chen, H., & Feng, M. (2015). Water Content and Oxygen Isotopic Composition of Alkali Basalts from the Taihang Mountains, China: Recycled Oceanic Components in the Mantle Source. *Journal of Petrology*, 0, 1–22. <https://doi.org/10.1093/petrology/egv013>

Liu, Y. Q., Kuang, H. W., Peng, N., Xu, H., Zhang, P., Wang, N. S., & An, W. (2015). Mesozoic basins and associated palaeogeographic evolution in North China. *Journal of Palaeogeography*, 4(2), 189–202. <https://doi.org/10.3724/SP.J.1261.2015.00073>

Louys, J. (2007). Limited effect of the Quaternary’s largest super-eruption (Toba) on land mammals from Southeast Asia. *Quaternary Science Reviews*,

26, 3018 3117. <https://doi.org/10.1016/j.quascirev.2007.09.008>

Martin, J. H., Coale, K. H., Johnson, K. S., Fitzwater, S. E., Gordon, R. M., Tanner, S. J., Hunter, C. N., Elrod, V. A., Nowicki, J. L., Coley, T. L., Barber, R. T., Lindley, S., Watson, A. J., Van Scoy, K., Law, C. S., Liddicoat, M. I., Llng, R., Stanton, T., Stockel, J., Collins, C., Anderson, A., Bidigare, R., Ondrusek, M., Latasa, M., Millero, F. J., Lee, K., Yao, W., Zhang, J. Z., Friederich, G., Sakamoto, C., Chavez, F., Buck, K., Kolber, Z., Greene, R., Falkowski, P., Chisholm, S. W., Hoge, F., Swift, R., Yungel, J., Turner, S., Nightingale, P., Hatton, A., Liss, P., & Tindale, N. W. (1994). Testing the iron hypothesis in ecosystems of the equatorial Pacific Ocean. *Nature*, *371*, 123 129. <https://doi.org/10.1038/371123a0>

Mather, T. A. (2015). Volcanoes and the environment: Lessons for understanding Earth's past and future from studies of present-day volcanic emissions. *Journal of Volcanology and Geothermal Research*, *304*, 160 179. <https://doi.org/10.1016/j.jvolgeores.2015.08.016>

Meng, X. Y., Kleinsasser, J. M., Richards, J. P., Tapster, S. R., Jugo, P. J., Simon, A. C., Kontak, D. J., Robb, L., Bybee, G. M., Marsh, J. H., & Stern, R. A. (2021). Oxidized sulfur-rich arc magmas formed porphyry Cu deposits by 1.88 Ga. *Nature Communications*, *12*, 2189. <https://doi.org/10.1038/s41467-021-22349-z>

Oppenheimer, C., Fischer, T. P., & Scaillet, B. (2014). Volcanic Degassing: Process and Impact. In Rudnick, R. L. (ed), *Treatise on Geochemistry, second ed.* (pp. 111 179). New York: Elsevier. <https://doi.org/10.1016/B978-0-08-095975-7.00304-1>

Pan, Y. H., Sha, J. G., Zhou, Z. H., & Fürsich, F. T. (2013). The Jehol Biota: Definition and distribution of exceptionally preserved relicts of a continental Early Cretaceous ecosystem. *Cretaceous Research*, *44*, 30 38. <https://doi.org/10.1016/j.cretres.2013.03.007>

Parat, F., & Holtz, F. (2004). Sulfur partitioning between apatite and melt and effect of sulfur on apatite solubility at oxidizing conditions. *Contributions to Mineralogy and Petrology*, *147*, 201 212. <https://doi.org/10.1007/s00410-004-0553-7>

Parat, F., Holtz, F., & Streck, M. J. (2011). Sulfur-bearing Magmatic Accessory Minerals. *Reviews in Mineralogy & Geochemistry*, *73*, 285 314. <https://doi.org/10.2138/rmg.2011.73.10>

Price, G. D., & Hart, M. B. (2002). Isotopic evidence for Early to mid-Cretaceous ocean temperature variability. *Marine Micropaleontology*, *46*, 45 58. [https://doi.org/10.1016/S0377-8398\(02\)00043-9](https://doi.org/10.1016/S0377-8398(02)00043-9)

Rudnick, R. L., & Gao, S. (2014). Composition of the Continental Crust. In Holland, H. D. and Turekian, K. K. (Eds.), *Treatise on Geochemistry, second*

- ed. (pp. 1 51). New York: Elsevier. <https://doi.org/10.1016/B978-0-08-095975-7.00301-6>
- Sobolev, S. V., Sobolev, A. V., Kuzmin, D. V., Krivolutskaya, N. A., Petrunin, A. G., Arndt, N. T., Radko, V. A., & Vasiliev, Y. R. (2011). Linking mantle plumes, large igneous provinces and environmental catastrophes. *Nature*, *477*, 312-318. <https://doi.org/10.1038/nature10385>
- Stock, M. J., Humphreys, M. C. S., Smith, V. C., Isaia, R., & Pyle, D. M. (2016). Late-stage volatile saturation as a potential trigger for explosive volcanic eruptions. *Nature Geoscience*, *9*, 249 254. <https://doi.org/10.1038/ngeo2639>
- Tatsumi, Y. (2008). Making continental crust: The sanukitoid connection. *Chinese Science Bulletin*, *53*, 1620 1633. <https://doi.org/10.1007/s11434-008-0185-9>
- Timmreck, C., Graf, H. F., Zanchettin, D., Hagemann, S., Kleinen, T., & Krüger, K. (2012). Climate response to the Toba super-eruption: Regional changes. *Quaternary International*, *258*, 30 44. <https://doi.org/10.1016/j.quaint.2011.10.008>
- Tyrrell, T. (1999). The relative influences of nitrogen and phosphorus on oceanic primary production. *Nature*, *400*, 525 531. <https://doi.org/10.1038/22941>
- Van Hoose, A. E., Streck, M. J., Pallister, J. S., & Wälle, M. (2013). Sulfur evolution of the 1991 Pinatubo magmas based on apatite. *Journal of Volcanology and Geothermal Research*, *257*, 72 89. <https://doi.org/10.1016/j.jvolgeores.2013.03.007>
- Vitousek, P. M., Porder, S., Houlton, B. Z., & Chadwick, O. A. (2010). Terrestrial phosphorus limitation: mechanisms, implications, and nitrogen–phosphorus interactions. *Ecological Applications*, *20*(1), 5 15. <https://doi.org/10.1890/08-0127.1>
- Wallace, P. J., Plank, T., Bodnar, R. J., Gaetani, G. A., & Shea, T. (2021). Olivine-Hosted Melt Inclusions: A Microscopic Perspective on a Complex Magmatic World. *Annual Review of Earth and Planetary Sciences*, *49*, 465 494. <https://doi.org/10.1146/annurev-earth-082420-060506>
- Wang, Q. F., Lu, H. N., & Yang, J. L. (2008). Charophytes. In Chang, M. M., Chen, P. J., Wang, Y. Q., Wang, Y., & Miao, D.S. (Eds.), *The Jehol Fossils: The Emergence of Feathered Dinosaurs, Beaked Birds and Flowering Plants* (pp. 162 165). Academic Press, Elsevier Ltd. <https://doi.org/10.1016/B978-012374173-8.50019-3>
- Wang, X. L., & Zhou, Z. H. (2008). Mesozoic Pompeii, In Chang, M. M., Chen, P. J., Wang, Y. Q., Wang, Y., & Miao, D.S. (Eds.), *The Jehol Fossils: The Emergence of Feathered Dinosaurs, Beaked Birds and Flowering Plants* (pp. 19 35). Academic Press, Elsevier Ltd. <https://doi.org/10.1016/B978-012374173-8.50003-X>
- Webster, J. D., & Piccoli, P. M. (2015). Magmatic Apatite: A Powerful, Yet Deceptive, Mineral. *Elements*, *11*, 177 182. <https://doi.org/10.2113/gselements.11.3.177>

- Wilson, T. M., Cole, J. W., Stewart, C., Cronin, S. J., & Johnston, D. M. (2011). Ash storms: impacts of wind-remobilised volcanic ash on rural communities and agriculture following the 1991 Hudson eruption, southern Patagonia, Chile. *Bulletin of Volcanology*, *73*, 223–239. <https://doi.org/10.1007/s00445-010-0396-1>
- Workman, R. K., Hauri, E. H., Hart, S. R., Wang, J. H., & Blusztajn, J. (2006). Volatile and trace elements in basaltic glasses from Samoa: Implications for water distribution in the mantle. *Earth and Planetary Science Letters*, *241*, 932–951. <https://doi.org/10.1016/j.epsl.2005.10.028>
- Wu, F. Y., Lin, J. Q., Wilde, S. A., Zhang, X. O., & Yang, J. H. (2005). Nature and significance of the Early Cretaceous giant igneous event in eastern China. *Earth and Planetary Science Letters*, *233*, 103–119. <https://doi.org/10.1016/j.epsl.2005.02.019>
- Wu, F. Y., Yang, J. H., Xu, Y. G., Wilde, S. A., & Walker, R. J. (2019). Destruction of the North China Craton in the Mesozoic. *Annual Review of Earth and Planetary Sciences*, *47*, 173–195. <https://doi.org/10.1146/annurev-earth-053018-060342>
- Wu, S. Q. (2008). Land Plants. In Chang, M. M., Chen, P. J., Wang, Y. Q., Wang, Y., & Miao, D. S. (Eds.), *The Jehol Fossils: The Emergence of Feathered Dinosaurs, Beaked Birds and Flowering Plants* (pp. 167–178). Academic Press, Elsevier Ltd. <https://doi.org/10.1016/B978-012374173-8.50020-X>
- Xia, Q. K., Liu, J., Liu, S. C., Kovács, I., Feng, M., & Dang, L. (2013). High water content in Mesozoic primitive basalts of the North China Craton and implication on the destruction of cratonic mantle lithosphere. *Earth and Planetary Science Letters*, *361*, 85–97. <https://doi.org/10.1016/j.epsl.2012.11.024>
- Yang, B., Collins, A. S., Cox, G. M., Jarrett, A. J. M., Denyszyn, S., Blades, M. L., Farkaš, J., & Glorie, S. (2020). Using Mesoproterozoic Sedimentary Geochemistry to Reconstruct Basin Geography and Link Organic Carbon Productivity to Nutrient Flux from a Northern Australia Large Igneous Province. *Basin Research*, *32*, 1734–1750. <https://doi.org/10.1111/bre.12450>
- Yang, F., Santosh, M., Kim, S. W., Zhou, H. Y., & Jeong, Y. J. (2019). Late Mesozoic intraplate rhyolitic volcanism in the North China Craton: Far-field effect of the westward subduction of the Paleo-Pacific Plate. *Geological Society of America Bulletin*, *132*(1/2), 291–309. <https://doi.org/10.1130/B35123.1>
- Yang, S. H., He, H. Y., Jin, F., Zhang, F. C., Wu, Y. B., Yu, Z. Q., Li, Q. L., Wang, M., O'Connor, J. K., Deng, C. L., Zhu, R. X., & Zhou, Z. H. (2020). The appearance and duration of the Jehol Biota Constraint from SIMS U-Pb zircon dating for the Huajiying Formation in northern China. *Proceedings of the National Academy of Sciences of the United States of America*, *117*, 14299–14305. <https://doi.org/10.1073/pnas.1918272117>
- Yang, X. J., Wang, Y. D., & Zhang, W. (2013). Occurrences of Early Cretaceous

fossil woods in China implications for paleoclimates. *Palaeogeography, Palaeoclimatology, Palaeoecology*, 385, 213–220. <https://doi.org/10.1016/j.palaeo.2013.05.019>

Yu, Z. Q., Wang, M., Li, Y. J., Deng, C. L., & He, H. Y. (2021). New geochronological constraints for the Lower Cretaceous Jiufotang Formation in Jianchang Basin, NE China, and their implications for the late Jehol Biota. *Palaeogeography, Palaeoclimatology, Palaeoecology*, 583, 110657. <https://doi.org/10.1016/j.palaeo.2021.110657>

Zhang, H., Liu, X. M., Gao, S., Zhang, L. J., Li, Z. T., Yang, F. L., & Wang, X. C. (2005). Redefinition of the Zhangjiakou Formation in Lingyuan, western Liaoning and its significance—Constraints from Laser ICP-MS zircon U-Pb ages (in Chinese with English abstract). *Geological Bulletin of China*, 24(2), 110–117.

Zhang, X. L., Zhang, G. J., & Sha, J. G. (2016). Lacustrine sedimentary record of early Aptian carbon cycle perturbation in western Liaoning, China. *Cretaceous Research*, 62, 122–129. <https://doi.org/10.1016/j.cretres.2015.10.001>

Zhong, Y. T., Huyskens, M. H., Yin, Q. Z., Wang, Y. Q., Ma, Q., & Xu, Y. G. (2021). High-precision geochronological constraints on the duration of ‘Dinosaur Pompeii’ and the Yixian Formation. *National Science Review*, 0, nwab063. <https://doi.org/10.1093/nsr/nwab063>

Zhou, L., Algeo, T. J., Feng, L. P., Zhu, R. X., Pan, Y. X., Gao, S., Zhao, L. S., & Wu, Y. B. (2016). Relationship of pyroclastic volcanism and lake-water acidification to Jehol Biota mass mortality events (Early Cretaceous, northeastern China). *Chemical Geology*, 428, 59–76. <https://doi.org/10.1016/j.chemgeo.2016.02.029>

Zhou, Z. H., Barrett, P. M., & Hilton, J. (2003). An exceptionally preserved Lower Cretaceous ecosystem. *Nature*, 421, 807–814. <https://doi.org/10.1038/nature01420>

Zhou, Z. H., Meng, Q. R., Zhu, R. X., & Wang, M. (2021). Spatiotemporal evolution of the Jehol Biota: Responses to the North China craton destruction in the Early Cretaceous. *Proceedings of the National Academy of Sciences of the United States of America*, 118, 1–7. <https://doi.org/10.1073/pnas.2107859118>

Zhou, Z. H. (2014). The Jehol Biota, an Early Cretaceous terrestrial Lagerstätte: new discoveries and implications. *National Science Review*, 1, 543–559. <https://doi.org/10.1093/nsr/nwu055>

Zhu, R. X., Zhou, Z. H., & Meng, Q. R. (2020). Destruction of the North China Craton and its influence on surface geology and terrestrial biotas (in Chinese with English abstract). *Chinese Science Bulletin*, 65, 2954–2965. doi: 10.1360/TB-2020-0219

### References From the Supporting Information

Black, B. A., Elkins-Tanton, L. T., Rowe, M. C., & Peate, I. U. (2012). Magnitude and consequences of volatile release from the Siberian Traps. *Earth and*

*Planetary Science Letters*, 317 318, 363 373. <https://doi.org/10.1016/j.epsl.2011.12.001>

Devine, J. D., Sigurdsson, H., Davis, A. N., & Self, S. (1984). Estimates of sulfur and chlorine yield to the atmosphere from volcanic eruptions and potential climatic effects. *Journal of Geophysical Research: Solid Earth*, 89, 6309 6325. <https://doi.org/10.1029/JB089iB07p06309>

Gerlach, T. M., Westrich, H. R., Casadevall, T. J., & Finnegan, D. L. (1994). Vapor saturation and accumulation in magmas of the 1989-1990 eruption of Redoubt Volcano, Alaska. *Journal of Volcanology and Geothermal Research*, 62, 317 337. [https://doi.org/10.1016/0377-0273\(94\)90039-6](https://doi.org/10.1016/0377-0273(94)90039-6)

Li, W. R. & Costa, F. (2020). A thermodynamic model for F-Cl-OH partitioning between silicate melts and apatite including non-ideal mixing with application to constraining melt volatile budgets. *Geochimica et Cosmochimica Acta*, 269, 203 222. <https://doi.org/10.1016/j.gca.2019.10.035>

Peccerillo, A. & Taylor, S. R. (1976). Geochemistry of Eocene Calc-Alkaline Volcanic Rocks from Kastamonu Area, Northern Turkey. *Contributions to Mineralogy and Petrology*, 58, 63 81. <https://doi.org/10.1007/BF00384745>

Piccoli, P. & Candela, P. (1994). Apatite in felsic rocks: a model for the estimation of initial halogen concentrations in the Bishop Tuff (Long Valley) and Tuolumne Intrusive suite (Sierra Nevada Batholith) magmas. *American Journal of Science*, 294, 92 135. <https://doi.org/10.2475/ajs.294.1.92>

Ridolfi, F., Renzulli, A., & Puerini, M. (2010). Stability and chemical equilibrium of amphibole in calc-alkaline magmas an overview, new thermobarometric formulations and application to subduction-related volcanoes. *Contributions to Mineralogy and Petrology*, 160, 45 66. <https://doi.org/10.1007/s00410-009-0465-7>

Sigurdsson, H., Carey, S., Palais, J. M., & Devine, J. (1990). Pre-eruption compositional gradients and mixing of andesite and dacite magma erupted from Nevado del Ruiz Volcano, Colombia in 1985. *Journal of Volcanology and Geothermal Research*, 41, 127 151. [https://doi.org/10.1016/0377-0273\(90\)90086-U](https://doi.org/10.1016/0377-0273(90)90086-U)

Vidal, C., Métrich, N., Komorowski, J. C., Pratomo, I., Michel, A., Kartadinata, N., Robert, V., & Lavigne, F. (2016). The 1257 Samalás eruption (Lombok, Indonesia): the single greatest stratospheric gas release of the Common Era. *Scientific Reports*, 6, 34868. <https://doi.org/10.1038/srep34868>

Westrich, H. R., Eichelberger, J. C., & Hervig, R. L. (1991). Degassing of the 1912 Katmai magmas. *Geophysical Research Letters*, 18, 1561 1564. <https://doi.org/10.1029/91GL01667>

Wones, D. R. & Eugster, H. P. (1965). Stability of biotite experiment, theory and application. *American Mineralogist*, 50, 1228 1272.